

Quantum anomalous Hall effect induced by circularly polarized light on samarium hexaboride surface

Udai Prakash Tyagi and *Partha Goswami

D.B.College, University of Delhi, Kalkaji, New Delhi-110019, India

Email of the first author: uptyagi@yahoo.co.in

**Email of the corresponding author: physicsgoswami@gmail.com*

Abstract

We consider a time-dependent, surface Hamiltonian for the 3D compound samarium hexaboride based on the slave boson protocol linked version of the periodic Anderson model reported earlier. We show the possible access to the quantum anomalous Hall state due to the normal incidence of circularly polarized light on the surface of the compound in the high frequency limit within the framework of the Floquet theory. The chern number is found to be unity for the right-handed as well as the left-handed circularly polarized light.

Keywords: Periodic Anderson model, Circularly polarized light, Floquet Theory, High-frequency limit, Chern number.

1.INTRODUCTION

The polarized terahertz radiation provides a potent modus operandi to carry out theoretical proposition and experimental realization, manipulation, and detection of diverse unconventional/novel electronic properties of materials, such as the realization of novel quantum phases like light induced quantum anomalous Hall (QAH) phase [1-3], the topological phase transitions in semi-metals [4-8], the Floquet engineering of magnetism in topological insulator thin films [9,10], and so on. The exotic Floquet topological phases with a high tunability could be realized using this highly efficient and promising platform. In fact, there has been an upsurge on experimental front in the search for topological states (which may be inaccessible in static systems), in solid state [11], ultra cold-atom [12], and optical systems [13] and so on through the periodic driving of polarized radiation. The circularly polarized radiation field (CPRF) is described by a time-periodic (time period $T = 2\pi/\omega$ where ω is the frequency of light) electromagnetic gauge field $\mathbf{A}(t)$. Once we have included a gauge field, it is necessary that we make the Peierls substitution which couples lattice electrons to the gauge field. Thus, in the presence of CPRF, the Hamiltonian of a system becomes periodic in time. One can now transform the time-dependent Hamiltonian problem to a time-independent one using the Floquet's theory [14-19]. Analogous to the Bloch theory, a solution for the time-dependent Schrodinger equation of the system is obtained involving the Floquet quasi-energy and the time-periodic Floquet state with the periodicity T . The Floquet state could be expanded in a Fourier series which makes us arrive at an infinite dimensional eigenvalue equation in the Sambe space [14]. In the Floquet-

Magnus limit [19], the system irradiated by the circularly polarized radiation can be described by an effective, static Hamiltonian.

The minimalistic bulk Hamiltonian of a topological Kondo insulator (TKI) SmB₆ is given in refs. [20-25]. This is a slave boson (SB) protocol related extended version of the periodic Anderson model (PAM) [22-24]. Our bulk Hamiltonian in ref. [23] (of SmB₆) involving d and f fermions (with the corresponding hopping integrals denoted by t_{d_1} and t_{f_1} , respectively) captured essential physics of TKI in the presence of the strong coulomb repulsion U_f ($U_f \gg t_{d_1}$) between f electrons on the same site, and the spin-orbit hybridization. The latter is the harbinger of a topological dispensation. In the references [22-24], a detailed exposition of PAM and SB formalism could be found. In the present paper, which is a sequel to that in ref. [23], we make use of the Floquet theory [14-19] to investigate the system surface interaction with the incident electromagnetic radiation in the high-frequency limit. For this purpose, we consider a low-energy time-dependent, surface Hamiltonian (H_f) – a variant of the extended PAM. This Hamiltonian has been obtained by the evanescent wave method. The slab-geometry method could equally well be applied. Interestingly, the radiation field leads to the possibility of the emergence of the quantum anomalous Hall (QAH) state as we find the integer values of the chern number C ($C = 1$) for different parameter windows.

The way we structure this paper is as follows: We obtain a low-energy version of the Floquet surface Hamiltonian in section 2. Upon using this Hamiltonian we discuss the possibility of the emergence of a novel phase due to the broken time reversal symmetry (TRS). In section 3, we calculate the eigenvalues and the corresponding eigenvectors of the surface Hamiltonian. We also present the corresponding band spectrum in this section. To gain further insight into the nature of this emergent phase we calculate the chern number in section 4. The communication ends with very brief concluding remarks in section 5.

2. MODEL

The periodic Anderson model (PAM) for a topological Kondo insulator SmB₆ involving d and f electrons is discussed in refs. [22-25]. In particular, refs. [23,24] present PAM, and its extension using the slave-boson (SB) protocol, in full glory. Upon following these references we write the

Hamiltonian matrix in k -space as $h(k, \mu, |b|) = \frac{\widetilde{E}_k^d(\mu, k)}{2} (I^{4 \times 4} + \gamma^0) + \frac{\widetilde{E}_k^f(\mu, |b|, k)}{2} (I^{4 \times 4} - \gamma^0) + \partial_\mu \gamma^0 \gamma^\mu$ in the basis $(d_{k,\uparrow} \ d_{k,\downarrow} \ |b|c_{k,\uparrow} \ |b|c_{k,\downarrow})^T$ straightway. We represent the creation (annihilation) operators by $d_{k,\tau}^\dagger (d_{k,\tau})$ and $f_{k,\tau}^\dagger = |b|c_{k,\tau}^\dagger (|b|c_{k,\tau})$, respectively, for d and f electrons. The index $\tau (= \uparrow, \downarrow)$ represents the spin (pseudo-spin) for d -(f -) electrons. The parameter ' b ' may be complex as the density distribution of the Bose-condensate is represented by a wavefunction with a well-defined amplitude and phase [23]. Here-in-after, we shall denote $|b|$ simply by the letter ' b '. The dispersions $\widetilde{E}_k^d(\mu, k) = -\mu + 3t_{d_1} - 3t_{f_1} - \mathfrak{h}_d$ and $\widetilde{E}_k^f(\mu, b, k) = -\mu - 3t_{d_1} - 3t_{f_1} + b^2(\epsilon_f + 6t_{f_1}) - \mathfrak{h}_f$, where $(\mathfrak{h}_d, \mathfrak{h}_f)$ are given in the Appendix A. The

symbol $I^{4 \times 4}$ is for the 4×4 identity matrix, μ is the chemical potential of the fermion number, and $\vartheta_\mu = (\vartheta_x, \vartheta_y, \vartheta_z)$, where $\vartheta_j = (2Vb \sin ak_j)$, $j = (x, y, z)$. The anti-commuting $(\frac{1}{2}\{\gamma^\mu, \gamma^\nu\} = g^{\mu\nu} I_{4 \times 4})$ matrices $(\gamma^0, \gamma^1, \gamma^2, \gamma^3, \gamma^5)$ are Dirac matrices in contravariant notations. We note that the γ^0 matrix is hermitian while the $(\gamma^1, \gamma^2, \gamma^3)$ matrices are anti-hermitian. The terms (t_{d1}, t_{f1}) , (t_{d2}, t_{f2}) , and (t_{d3}, t_{f3}) , respectively, are the NN , NNN , and $NNNN$ hopping parameters for d and f electrons; ϵ_f is the onsite energy of the f electrons and $a = 0.413$ nm is the crystal structure lattice constant of SmB_6 bulk. The system shows the bulk metallic as well as the bulk insulating phases are determined by the sign of t_{f1} . It is positive for the former and negative for the latter phase [22-25]. The negative sign of t_{f1} is also necessary for the band inversion, which induces the topological state [22-25]. Throughout the paper, we choose t_{d1} to be the unit of energy. Furthermore, it is straightforward to show that, without spin-orbit interactions, the Anderson Model is both time-reversal symmetric and inversion symmetric.

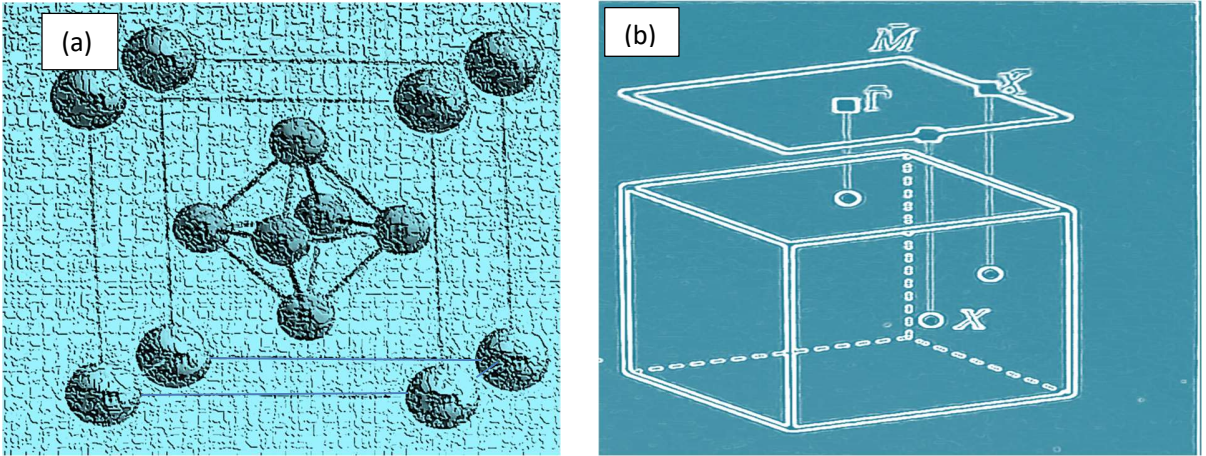


Figure 1. (a) A diagrammatic representation of SmB_6 crystal structure (with cubic lattice constant $a = 0.413$ nm). The Sm ions are located at the corners and the B_6 octahedron at the center of the cubic lattice. **(b)** The high symmetry points of the bulk Brillouin zone (BZ) are $\Gamma(0,0,0)$, $X\{(\pi, 0, 0), (0, \pi, 0), (0, 0, \pi)\}$, $M\{(\pi, \pi, 0), (\pi, 0, \pi), (0, \pi, \pi)\}$ and $R(\pi, \pi, \pi)$. The projection of the X points in the (001) surface BZ gives the points $\bar{\Gamma}(0,0)$ and $\bar{X}(\pi, 0)$.

In order to obtain surface Hamiltonian $H_f(k_x, k_y, \mu, b)$, earlier [22,24] we have adopted the method involving the slab-geometry considering a set of orthonormal basis states. For the sake of brevity and simplicity we lean on the heuristic evanescent wave approach (EWA) [23,26] given in the Appendix A. The slab geometry approach (SGA) is another way to obtain surface states. We treat the model Hamiltonian matrix in (1) in the low-energy limit near $\bar{\Gamma}(0,0)$ point. As shown in the appendix A, the low-energy surface Hamiltonian can now be conveniently written as $H_f = \frac{\epsilon(k,d,\mu,b) + \vartheta(k,b,d)}{2} (I^{4 \times 4} + \gamma^0) + \frac{\epsilon(k,d,\mu,b) - \vartheta(k,b,d)}{2} (I^{4 \times 4} - \gamma^0) + iA_1 a k_x \gamma^2 + A_1 a k_y \gamma^0 \gamma^2 - iA_1 \left(\frac{a}{d}\right) \gamma^3$, where $A_1 = 2Vb$. In this limit, the functions $\epsilon(k, \mu, d, b) = \frac{(\widetilde{E}_k^d(\mu, k) + \widetilde{E}_k^f(\mu, b, k))}{2}$ and

$\vartheta(k, \mu, d, b) = \frac{(\widetilde{E}_k^d(\mu, k) - \widetilde{E}_k^f(\mu, b, k))}{2}$ have been approximated to $O(a^2 k^2)$. These functions are given in Appendix A.

We now assume the normal incidence of CPRF on the surface SmB_6 . Suppose the angular frequency of the radiation field incident on the surface is $\omega \sim 10^{15} \text{radian} - s^{-1}$, the period $T = 2\pi/\omega \sim 10^{-15} \text{ s}$, and wavelength $\lambda_{in} \approx 1500 \text{ nm}$. Therefore the ratio of the penetration depth (d) and the wavelength (λ_{in}) is much smaller than unity. The radiation field $\mathbf{E}(t)$ may be expressed in terms of the electric scalar potential (assumed to be zero) and the time-varying magnetic vector potential $\mathbf{A}(t) = \mathbf{A}(t + T) = \mathbf{A}_0(\sin(\omega t), \sin(\omega t + \psi), 0)$ through the relation: $\mathbf{E}(t) = -\frac{\partial \mathbf{A}(t)}{\partial t} = -\mathbf{E}(\cos(\omega t), \cos(\omega t + \psi), 0)$, $\mathbf{E} = \mathbf{A}_0 \omega$. In particular, when the phase $\psi = 0$ or π , the radiation field is linearly polarized. When $\psi = \frac{\pi}{2}$ ($\psi = -\frac{\pi}{2}$), the radiation field is left-handed (right-handed) circularly polarized. Upon taking the electromagnetic field into consideration the Hamiltonian $H_f(k_x, k_y, \mu, b)$ becomes time dependent. Once we have included a gauge field, it is necessary that we make the Peierls substitution $H(\mathbf{k}, t, b) = H_f\left(\mathbf{k} - \frac{e}{\hbar} \mathbf{A}(t), b\right)$. The quantity $I = (aA_0)^2 = \left(\frac{aeE}{\hbar\omega}\right)^2$ corresponds to the dimensionless radiation intensity. Now the Floquet theory [14-19] can be applied to our time-periodic Hamiltonian $H_f(t) = H_f(t + T)$ to obtain a static effective Hamiltonian $H_f(k, d, aA_0, \mu, b)$. The details have been presented in the Appendix B. We have shown that, only when the incident radiation field is left-(or, right-) handed circularly polarized, the time reversal symmetry (TRS) is broken by $H_f(k, q, aA_0, b)$. Another possible way of visualizing TRS breaking will be to write the Hamiltonian $H_f(k, q, aA_0, b)$ in the basis $(d_{k,\uparrow} \ d_{k,\downarrow} \ bc_{k,\uparrow} \ bc_{k,\downarrow})^T$. We obtain

$$H_f = \epsilon_{OP} I^{4 \times 4} + \frac{\vartheta_{OP}^+ + \vartheta_{OP}^-}{2} \gamma^0 + 2C_\mu \Sigma^\mu + A_{1OP}^+ ak_y \frac{\gamma^0 \gamma^2 - i\gamma^1}{2} + A_{1O}^- ak_y \frac{\gamma^0 \gamma^2 + i\gamma^1}{2} \\ + A_{1OP}^+ ak_x \frac{\gamma^0 \gamma^1 + i\gamma^2}{2} - A_{1OP}^- ak_x \frac{\gamma^0 \gamma^1 - i\gamma^2}{2} + \frac{i(A_{1OP}^- - A_{1OP}^+)aq}{2} \gamma^0 \gamma^5 - \frac{i(A_{1OP}^- + A_{1OP}^+)aq}{2} \gamma^3, \quad (1)$$

where $C_\mu = \left(0, 0, M = \frac{\vartheta_{OP}^+ - \vartheta_{OP}^-}{2}\right)$, $\Sigma^\mu = \left(\frac{1}{2}\right) \epsilon^{\mu\nu\rho} \sigma_{\nu\rho}$, $q = d^{-1}$, and $\sigma_{\nu\rho} = \left(\frac{i}{2}\right) [\gamma_\nu, \gamma_\rho]$. Given the Dirac matrices obeying the anticommutation relations mentioned above, we may define the spin matrices as $\frac{1}{2} \sigma^{\nu\rho}$. It may be noted that these matrices obey the same commutation relations as the generators $J^{\mu\nu}$ of the continuous Lorentz group. Moreover, the commutation relations of $J^{\mu\nu}$ with a Lorentz vector are similar to the commutators $[\frac{1}{2} \sigma^{\nu\rho}, \gamma^\mu]$. As a matter of fact, all such four-band models could be written out in terms of the Dirac matrices. This Hamiltonian is presented in the alternative basis $(d_{k,\uparrow} \ bc_{k,\downarrow} \ d_{k,\downarrow} \ bc_{k,\uparrow})^T$ in the appendix A. Equation (1) or the one in the alternative basis in the appendix A is our model surface Hamiltonian periodically driven by polarized radiation. The functions $\epsilon_{OP} = \epsilon_{OP}(k, q, \mu, b)$, A_{1OP}^\pm , and $\vartheta_{OP}^\pm = \vartheta_{OP}^\pm(k, q, b)$ are defined below:

$$\epsilon_{OP}(k, q, \mu, b) = \epsilon_0(\mu, b) - D_1(b)a^2q^2 + D_2(b)a^2k^2 + a^2A_0^2D_2(b) + O(a^4k^4), \quad (2)$$

$$\vartheta_{OP}^{\pm}(k, q, b) = \vartheta_0(b) - B_1(b)a^2q^2 + B_2(b)a^2k^2 - \left(a^2A_0^2B_2 \pm \left(\frac{a^2A_0^2}{\hbar\omega}\right)\sin\psi A_1^2\right), \quad (3)$$

$$A_{1OP}^{\pm} = A_1 \left(1 \pm 2B_2\sin\psi \left(\frac{a^2A_0^2}{\hbar\omega}\right)\right), A_1 = 2Vb, C_3 = M = [-2\left(\frac{a^2A_0^2}{\hbar\omega}\right)\sin\psi A_1^2]. \quad (4)$$

Along with the off-diagonal terms, now the diagonal (mass) terms $[\frac{\vartheta_{OP}^+ + \vartheta_{OP}^-}{2}\gamma^0 + 2C_{\mu}\Sigma^{\mu}]$, dependent on the intensity and the polarization of radiation, appear in the Hamiltonian which implies that the system is now without the chiral symmetry. An immediate consequence of which is the possibility of tunable spin-polarization to be discussed elsewhere. Moreover, we notice from Eq.(2)-(4) (and the appendix A) that CPRF not only renormalizes terms involving d and f electron hopping integrals but also does the renormalization of the hybridization parameter(HP). The term $C_3 = M$ acts as the pseudo-magnetic exchange energy responsible for breaking the time reversal invariance.

The term $C_3 = M$ in (1) depends on the intensity and frequency of the incident radiation and the hybridization parameter. The modulation of this emergent pseudo-magnetization is possible by circularly polarized radiation field (CPRF): it increases with intensity of the incident radiation and decreases with the frequency. Since $\psi = \frac{\pi}{2}$ ($\psi = -\frac{\pi}{2}$), corresponds to the left-handed (right-handed) CPRF, we have $M < 0$ for the former and $M > 0$ for the latter. The latter case corresponds to the parallel spin configuration (pseudo-ferromagnetism) while the former to the anti-parallel one(pseudo-antiferromagnetism). Thus, the incidence of the CPRF on the SmB_6 surface would give rise to quantum anomalous Hall (QAH) state provided we show that the Chern number (C), associated with anomalous Hall conductivity (AHC), has integer values in this case. In the next section, we calculate the energy eigenvalues and the corresponding eigenvectors of the matrix (1). resulting from the interaction with radiation. We calculate the Chern number C in the section 4.

3. SURFACE STATE

The single-particle excitation spectrum (SPES) and the spectral gap, representing allowed energy values for electron in a system, are central feature to investigate as they provide important insights into the understanding the system. The eigenvalues (E_{α}) of the matrix (1), given by the quartic below, gives us SPES of the system driven periodically by the polarized radiation:

$$E_{\alpha}^4 + \gamma_{10}(k, b) E_{\alpha}^3 + \gamma_{20}(k, b) E_{\alpha}^2 + \gamma_{30}(k, b) E_{\alpha} + \gamma_{40}(k, b) = 0 \quad (\alpha = 1, 2, 3, 4) \quad (6)$$

where the coefficients $\gamma_{\alpha OP}(k, b)$ ($\alpha = 1, 2, 3, 4$) of the quartic are given by

$$\gamma_{10} = -\sum_{\alpha} \epsilon_{\alpha}, \gamma_{20} = \sum_{\mu \neq \nu} \epsilon_{\mu} \epsilon_{\nu} - (A_{1OP}^+ + A_{1O}^-)(aq)^2 - (A_{1O}^{+2} + A_{1OP}^{-2})(ak)^2, \quad (7)$$

$$\begin{aligned} \gamma_{30}(k, b) = & -(\epsilon_1 + \epsilon_2)\epsilon_3\epsilon_4 - (\epsilon_3 + \epsilon_4)\epsilon_1\epsilon_2 + (\epsilon_1 + \epsilon_2)A_{1OP}^{-2}(ak)^2 + (\epsilon_3 + \epsilon_4)A_{1OP}^{+2}(ak)^2 \\ & + (\epsilon_1 + \epsilon_4)A_{1O}^{-2}(aq)^2 + (\epsilon_2 + \epsilon_3)A_{1OP}^{+2}(aq)^2, \quad (8) \end{aligned}$$

$$\gamma_{40}(k) = \prod_{\mu} \epsilon_{\mu} - A_{1OP}^{-2}(ak)^2(\epsilon_1\epsilon_2) - A_{1OP}^{+2}(ak)^2(\epsilon_3\epsilon_4) + A_{1OP}^{-2}A_{1OP}^{+2}(ak)^4 + A_{1OP}^{-2}A_{1OP}^{+2}(aq)^4$$

$$-A_{10P}^{-2}(aq)^2(\epsilon_1\epsilon_4) - A_{10P}^{+2}(aq)^2(\epsilon_2\epsilon_3) - 2A_{10P}^{-2}A_{10P}^{+2}(aq)^2((ak_x)^2 - (ak_y)^2), \quad (9)$$

and

$$\epsilon_1 = \epsilon_{OP} + \vartheta_{OP}^+, \epsilon_2 = \epsilon_{OP} - \vartheta_{OP}^+, \epsilon_3 = \epsilon_{OP} + \vartheta_{OP}^-, \epsilon_4 = \epsilon_{OP} - \vartheta_{OP}^-. \quad (10)$$

The functions $\epsilon_{OP} = \epsilon_{OP}(k, q, \mu, b)$, A_{10P}^\pm , and $\vartheta_{OP}^\pm = \vartheta_{OP}^\pm(k, q, b)$ are defined by Eqs. (2)-(4). In view of the Ferrari's solution, we find the roots of the quartic in (6) as

$$E_\alpha(s, l, k, q, b, I) = s \sqrt{\frac{\eta_{OP}(k)}{2} - \frac{\gamma_{10P}(k, b)}{4}} + l \left(b_{OP}(k) - \left(\frac{\eta_{OP}(k)}{2} \right) + s c_{OP}(k) \sqrt{\frac{2}{\eta_{OP}(k)}} \right)^{\frac{1}{2}}. \quad (11)$$

where $\alpha = 1, 2, 3, 4$, $s = \pm 1$ is the spin index and $l = \pm 1$ is the band-index. The spin-up(down) ($s = \pm 1$) conduction band ($l = +1$), and the spin-up (down) ($s = \pm 1$) valence bands ($l = -1$), are denoted, respectively, by $E_1(l = +1, s = +1, k, b, I)$, $E_2(l = +1, s = -1, k, b, I)$, $E_3(l = -1, s = +1, k, b, I)$, and $E_4(l = -1, s = -1, k, b, I)$. The functions appearing in Eq. (10) are given by

$$\eta_{OP}(k) = \frac{2b_{OP}(k)}{3} + (\Delta_{OP}(k) - \Delta_{00}(k))^{\frac{1}{3}} - (\Delta_{OP}(k) + \Delta_{00}(k))^{\frac{1}{3}}, \quad (12)$$

$$\Delta_{00P}(k) = \left(\frac{b_{OP}^3(k)}{27} - \frac{b_{OP}(k)d_{OP}(k)}{3} - c_{OP}^2(k) \right),$$

$$\Delta_{OP}(k) = \left(\frac{2}{729} b_{OP}^6 + \frac{4d_{OP}^2 b_{OP}^2}{27} + c_{OP}^4 - \frac{d_{OP} b_{OP}^4}{81} - \frac{2b_{OP}^3}{27} + \frac{2c_{OP}^2 b_{OP} d_{OP}}{3} + \frac{d_{OP}^3}{27} \right)^{1/2}, \quad (13)$$

$$b_{OP}(k) = \left\{ \frac{3\gamma_{10P}(k, b)^2 - 8\gamma_{20P}(k, b)}{16} \right\}, \quad c_{OP}(k) = \left\{ \frac{-\gamma_{10P}(k, b)^3 + 4\gamma_{10P}(k, b)\gamma_{20P}(k, b) - 8\gamma_{30P}(k, b)}{32} \right\}, \quad (14)$$

$$d_{OP}(k) = \frac{-3\gamma_{10P}(k, b)^4 + 256\gamma_{40P}(k, b) - 64\gamma_{10P}(k, b)\gamma_{30P}(k, b) + 16\gamma_{10}(k, b)^2\gamma_{20P}(k, b)}{256}. \quad (15)$$

As noted in section 2, the quantity $I = (aA_0)^2 = \left(\frac{aeE}{\hbar\omega} \right)^2$ corresponds to the dimensionless radiation intensity. In order to obtain the eigenvalues of Eq. (1) when the intensity of the incident radiation is equal to zero, we simply need to put $I = (aA_0)^2 = 0$ in Eq. (11). We have plotted these eigenvalues in ref.[23] as a function of the dimensionless wavenumber. The graphical representations of the four-band spectrum showed the Dirac point feature at $\mathbf{k} = (0, 0)$, $(\pm 1, 0)$, and $(0, \pm 1)$. This is in agreement with the seminal work of Lu et al.[27]. On a quick side note, as discussed in the appendix A (Eq. (A.8)), we are able to present the Hamiltonian (1) in the block-diagonal form in a certain case. We shall focus presently on the non-block diagonal form given by (1).

The graphical representations in Figure 1 correspond to the energy eigenvalues $E_\alpha(s, \mathbf{k}, b, I)$ plotted as function of the wave number. These plots are obtained using a low energy Hamiltonian in our calculation around the $\bar{\Gamma}$ point. A band gap is the central requirement for QAH to exist. There is tiny band-gap at the $\bar{\Gamma}$ point between the bands closer to the chemical potential $\mu = 0$ as in Figures 1(a) (for the left-handed CPRF with $aA_0 = 0.95$) and 1(b) (for the right-handed CPRF with $aA_0 = 0.95$). In Figure 1(c) and 1(d) we have once again the plots of the energy eigenvalues as function of the wave number for $aA_0 = 0.35$ for the left-handed CPRF and the right-handed CPRF, respectively. These two figures clearly show that the required band gap does not appear when the intensity of the radiation is at a lower value. The gap opening and closing are clearly demonstrated in the insets in Figures 1(a)–(d). In Figures (c) and (d), apart from the valence/ the conduction band near degeneracy, the conduction band is a tad partially filled. This means, for the lower intensity of the incident radiation, the surface state is conducting, while the gap opening occurs only at the higher intensity. The Figures 1(e) and 1(f) represent the two-dimensional plots of the surface band spectrum for the plane polarized radiation. While the lower intensity plot (Figure 1(e)) is similar to that in 1(c) and 1(d), the figure 1(f) displays avoided crossing and corresponds to the higher intensity. The other parameter values used are $t_{d_1} = 1$, $t_{f_1} = -0.95$, $t_{d_2} = 0.01$, $t_{f_2} = 0.01$, $t_{d_3} = 0.001$, $t_{f_3} = 0.001$, $\epsilon_f = -0.02$, $V = 0.30$, $b = 0.91$, $q = 0.10$, and $\mu = 0$. Our graphical representations lead to the fact that, due to the light-matter interaction, the emergent unconventional phase corresponds to a novel state with gap opening or avoided crossing depending on the intensity of the incident radiation.

The surface states linked to the energy eigenvalues in (11) could be written as $|u^{(\alpha)}(\mathbf{k})\rangle = N_\alpha^{-\frac{1}{2}} \phi_\alpha(k)$, where $N_\alpha = [\psi_1^{(\alpha)*}(k)\psi_1^{(\alpha)}(k) + \psi_2^{(\alpha)*}(k)\psi_2^{(\alpha)}(k) + \psi_3^{(\alpha)*}(k)\psi_3^{(\alpha)}(k) + \psi_4^{(\alpha)*}(k)\psi_4^{(\alpha)}(k)]$, and $\phi_\alpha(k)$ is the transpose of the row vector $(\psi_1^{(\alpha)}(k) \ \psi_2^{(\alpha)}(k) \ \psi_3^{(\alpha)}(k) \ \psi_4^{(\alpha)}(k))$, $\alpha = 1, 2, 3, 4$. The elements $\psi_j^{(\alpha)}(k)$ are given by $\psi_1^{(\alpha)}(k) = Y_1^{(\alpha)} + iY_2^{(\alpha)}$, $\psi_2^{(\alpha)}(k) = \kappa_1^{(\alpha)} + i\kappa_2^{(\alpha)}$, $\psi_3^{(\alpha)}(k) = \Delta_1^{(\alpha)} + i\Delta_2^{(\alpha)}$, and $\psi_4^{(\alpha)}(k) = \mathcal{Q}^{(\alpha)} + i0$, where for the α^{th} band

$$Y_1^{(\alpha)} = \{-A_{10P}^+ A_{10P}^{-2} ((aq)^2 (ak_x) + (ak)^2 (ak_x)) + A_{10P}^+ (ak_x) (E_\alpha - \varepsilon_3)(E_\alpha - \varepsilon_4)\}, \quad (16)$$

$$Y_2^{(\alpha)} = \{-A_{10P}^+ A_{10P}^{-2} ((aq)^2 (ak_y) - (ak)^2 (ak_y)) - A_{10P}^+ (ak_y) (E_\alpha - \varepsilon_3)(E_\alpha - \varepsilon_4)\}, \quad (17)$$

$$\kappa_1^{(\alpha)} = \{-2A_{10P}^- A_{10P}^{+2} (aq)(ak_x)(ak_y)\}, \quad (18)$$

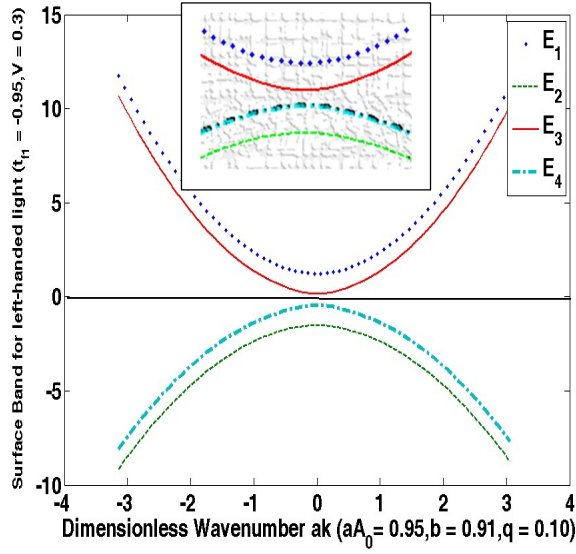
$$\kappa_2^{(\alpha)} = \{A_{10P}^- (aq)(E_\alpha - \varepsilon_1)(E_\alpha - \varepsilon_4) - A_{10P}^- A_{10P}^{+2} (aq)^3 - A_{10P}^- A_{10P}^{+2} (aq)(a^2 k_x^2 - a^2 k_y^2)\}, \quad (19)$$

$$\Delta_1^{(\alpha)} = \{A_{10P}^-^2 (E_\alpha - \varepsilon_1) + A_{10P}^+^2 (E_\alpha - \varepsilon_3)\} (aq)(ak_y), \quad (20)$$

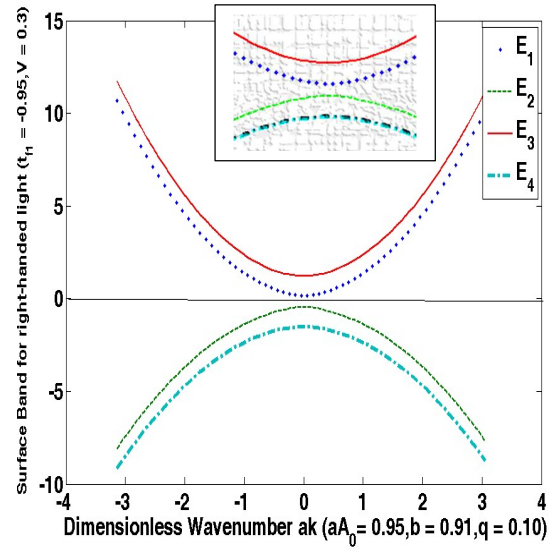
$$\Delta_2^{(\alpha)} = \{-A_{10P}^-^2 (E_\alpha - \varepsilon_1) + A_{10P}^+^2 (E_\alpha - \varepsilon_3)\} (aq)(ak_x), \quad (21)$$

$$\mathbb{Q}^{(\alpha)} = (E_\alpha - \varepsilon_1)(E_\alpha - \varepsilon_3)(E_\alpha - \varepsilon_4) - A_{10}^{-2} (a^2 k_x^2 + a^2 k_y^2) (E_\alpha - \varepsilon_1) - A_{10P}^{+2} (aq)^2 (E_\alpha - \varepsilon_3). \quad (22)$$

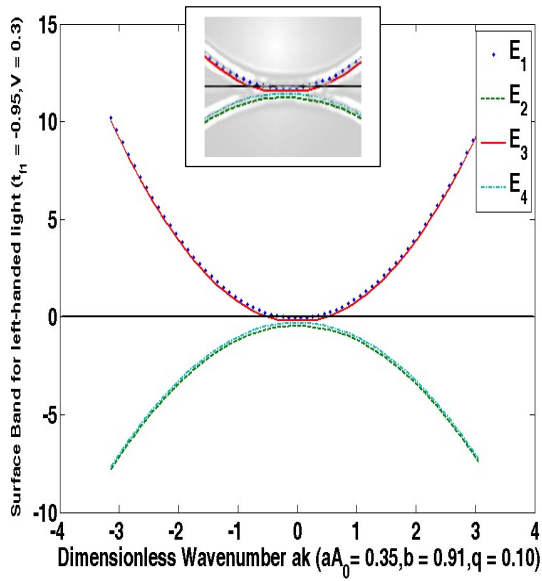
Here $N_\alpha = \gamma_1^{(\alpha)^2} + \gamma_2^{(\alpha)^2} + \kappa_1^{(\alpha)^2} + \kappa_2^{(\alpha)^2} + \Delta_1^{(\alpha)^2} + \Delta_2^{(\alpha)^2} + \mathbb{Q}^{(\alpha)^2}$. The calculation of eigenstate is the first step to obtain BC. In the next section we calculate the Chern number (C) linked to the Berry phase concept and provide evidence that the emergent novel state is could be the quantum anomalous Hall (QAH) phase.



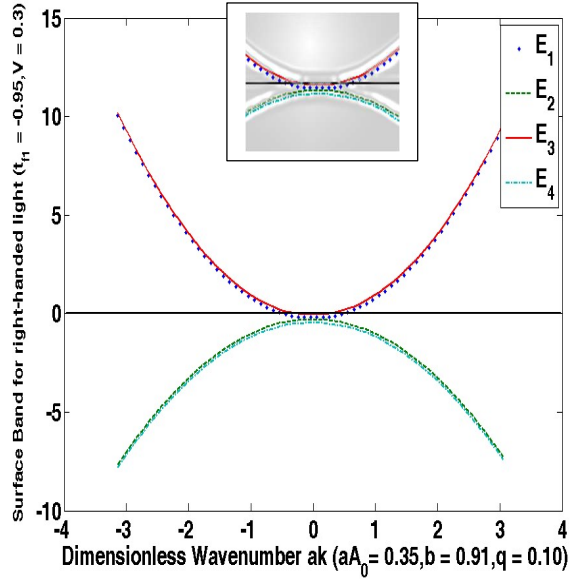
(a)



(b)



(c)



(d)

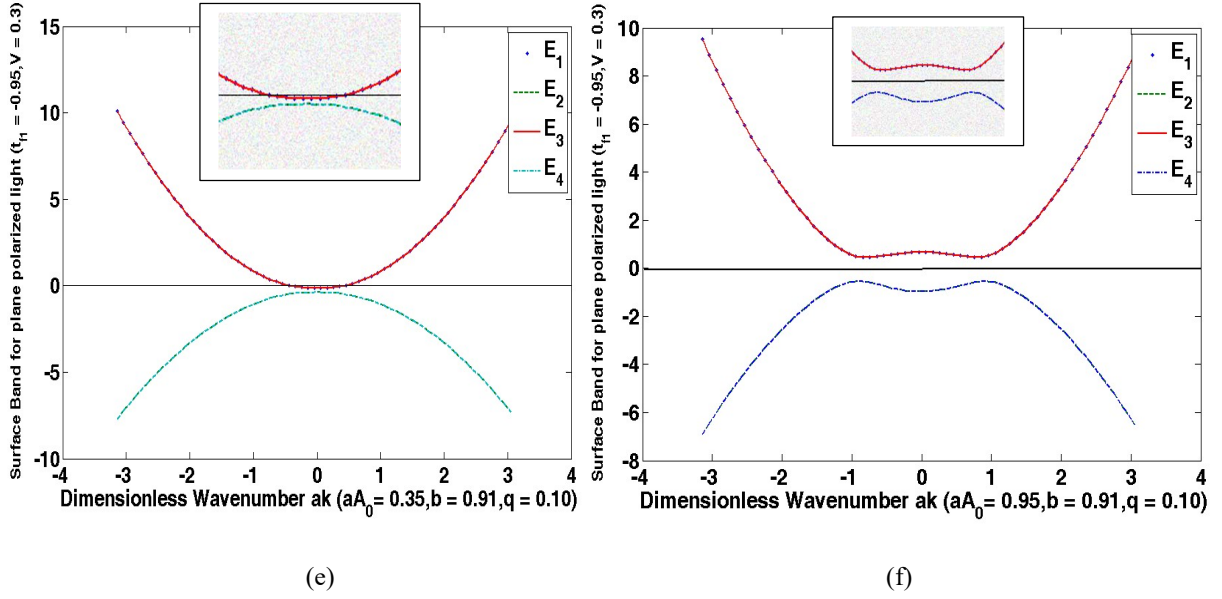


Figure 2. The 2D surface band plots above correspond to the energy eigenvalues $E_\alpha(s, \mathbf{k}, b, I)$ as function of the wave number. The insets represent the plots around the $\bar{\Gamma}$ point. **(a)((b))** $aA_0 = 0.95$ and the left-handed (right-handed) circularly polarized light. **(c)((d))** $aA_0 = 0.35$ and the left-handed (right-handed) circularly polarized light. The corresponding insets show gap opening and closing. **(e), (f)** The two-dimensional surface band plots for the plane polarized light. The figure (f) shows avoided crossing. The parameter values are $t_{d1} = 1, t_{f1} = -0.95, t_{d2} = 0.01, t_{f2} = 0.01, t_{d3} = 0.001, t_{f3} = 0.001, \epsilon_f = -0.02, V = 0.30, b = 0.91, q = 0.10$, and $\mu = 0$.

4. Quantum anomalous Hall effect

We have seen above that, through the periodic driving of polarized radiation, we are able to unlock a new route towards the possible engineering of the quantum anomalous Hall effect (QAHE) due to the presence of the term $C_3 = M \left[-2 \left(\frac{a^2 A_0^2}{\hbar \omega} \right) \sin \psi A_1^2 \right] \neq 0$. The term acts as the pseudo-magnetic exchange integral. To bolster the possibility of AHE, we calculate the Berry curvature (BC) and the Chern number below.

In the absence of external magnetic fields, the phenomenon of QAHE is largely governed by BC. A transverse velocity to the carrier electrons contributes to QAHE. We consider our case of the four-level system, the Hamiltonian of the system is given by (1) and the normalized eigenstates $|u^{(\alpha)}(\mathbf{k})\rangle$ given by (16) to calculate the anomalous Hall conductivity (AHC). The expression of AHC is $\sigma_{AH} = -\left(\frac{e^2}{h}\right) \sum_{\alpha \in \text{occupied}} \int_{BZ} \frac{d^2 k}{(2\pi)^3} f(E_\alpha(k) - \mu) \Omega_\alpha^z(\mathbf{k})$, where μ is the chemical potential of the fermion number, α is the occupied band index, $f(E_\alpha(k) - \mu)$ is the Fermi-Dirac distribution function and $\Omega_\alpha^z(k)$ is the z -component of the Berry curvature (BC) for the α^{th} occupied band. To obtain AHC, we calculate first BC using the Kubo formula [28,29]

$$\Omega_\alpha^z(k) = -2 \left[\text{Im} \sum_{\beta \neq \alpha} (E_\alpha(k) - E_\beta(k))^{-2} \left\langle u^{(\alpha)}(\mathbf{k}) \left| \frac{\partial H_f}{\partial k_x} \right| u^{(\beta)}(\mathbf{k}) \right\rangle \left\langle u^{(\beta)}(\mathbf{k}) \left| \frac{\partial H_f}{\partial k_y} \right| u^{(\alpha)}(\mathbf{k}) \right\rangle \right]. \quad (23)$$

where $H_f = H_f(k, q, aA_0, b)$ in (1). The energy eigenvalues in (11) and the corresponding eigenstates are also dependent on the same set of parameters (q, aA_0, b) . In the zero-temperature limit, we obtain $\sigma_{AH} = C \left(\frac{e^2}{h} \right)$ where $C = \sum_{\alpha} C_{\alpha}$, $C_{\alpha} = \int_{\text{BZ}} \Omega_j^z(k) \frac{d^2k}{(2\pi)^2}$. Here C is the Chern number, a topological invariant (an integer), also known as the Thouless-Kohmoto-Nightingale-Nijs (TKNN) number [30,31]. To simplify (24), we refer to the Heisenberg equation of motion $i\hbar \frac{d\hat{x}}{dt} = [\hat{x}, \hat{H}]$. In view of this equation, we find that the identity $\hbar \langle u^{(\alpha)}(k') | \hat{v}_j | u^{(\beta)}(k) \rangle = (E_{\alpha}(k') - E_{\beta}(k)) \left\langle u^{(\alpha)}(k') \left| \frac{\partial}{\partial k_j} \right| u^{(\beta)}(k) \right\rangle$ is satisfied for a system in a periodic potential and its Bloch states as the eigenstates $|u^{(\alpha)}(k)\rangle$. Here the operator $\hbar^{-1} \frac{\partial H_f}{\partial k_j} = \hat{v}_j$ represents the velocity in the $j = (x, y)$ direction. The Berry curvature $\Omega_j(\mathbf{k})$ is the analogue of the magnetic field in momentum-space with the Berry connection $A_j(\mathbf{k})$ acting as a vector potential; that is, $\nabla_{\mathbf{k}} \times \mathbf{A}_j(\mathbf{k}) = \Omega_j(\mathbf{k})$. Upon using the identity above, the z-component of BC may be written in the form as

$$\Omega_{xy}(k) = \sum_{\alpha} \left(\frac{\partial A_{\alpha,y}}{\partial k_x} - \frac{\partial A_{\alpha,x}}{\partial k_y} \right) = -2 \sum_{\alpha} \text{Im} \left\langle \frac{\partial u^{(\alpha)}(k)}{\partial k_x} \left| \frac{\partial u^{(\alpha)}(k)}{\partial k_y} \right\rangle. \quad (24)$$

It is not difficult to see that for the present problem the imaginary part of $\left\langle \frac{\partial u^{(\alpha)}(k)}{\partial k_x} \left| \frac{\partial u^{(\alpha)}(k)}{\partial k_y} \right\rangle$ is given by $\text{Im}(C_{x,1}C_{y,1}^{\dagger} - C_{x,2}C_{y,1}^{\dagger} - C_{x,1}C_{y,2}^{\dagger} + C_{x,2}C_{y,2}^{\dagger})$ where in view of Eq. (16)-(23) we obtain

$$C_{x,1} = N_{\alpha}^{-\frac{1}{2}} (\partial_x Y_1^{(\alpha)} - i \partial_x Y_2^{(\alpha)} \quad \kappa_1^{(\alpha)} - i \kappa_2^{(\alpha)} \quad \Delta_1^{(\alpha)} - i \Delta_2^{(\alpha)} \quad \mathcal{Q}^{(\alpha)}), \quad (25)$$

$$C_{y,1}^{\dagger} = N_{\alpha}^{-\frac{1}{2}} (\partial_y Y_1^{(\alpha)} - i \partial_y Y_2^{(\alpha)} \quad \kappa_1^{(\alpha)} - i \kappa_2^{(\alpha)} \quad \Delta_1^{(\alpha)} - i \Delta_2^{(\alpha)} \quad \mathcal{Q}^{(\alpha)})^{\dagger}, \quad (26)$$

$$C_{x,2} = 2^{-1} N_{\alpha}^{-\frac{3}{2}} \partial_x N_{\alpha} (Y_1^{(\alpha)} - i Y_2^{(\alpha)} \quad \kappa_1^{(\alpha)} - i \kappa_2^{(\alpha)} \quad \Delta_1^{(\alpha)} - i \Delta_2^{(\alpha)} \quad \mathcal{Q}^{(\alpha)}), \quad (27)$$

$$C_{y,2}^{\dagger} = 2^{-1} N_{\alpha}^{-\frac{3}{2}} \partial_y N_{\alpha} (Y_1^{(\alpha)} - i Y_2^{(\alpha)} \quad \kappa_1^{(\alpha)} - i \kappa_2^{(\alpha)} \quad \Delta_1^{(\alpha)} - i \Delta_2^{(\alpha)} \quad \mathcal{Q}^{(\alpha)})^{\dagger}. \quad (28)$$

The symbol ∂_x (∂_y) above stands for the differential coefficient $\frac{\partial}{\partial k_x}$ ($\frac{\partial}{\partial k_y}$). As it is clear from (27) and (28) that $(C_{x,2}C_{y,2}^{\dagger})$ is real, we need to find basically $\text{Im}(C_{x,1}C_{y,1}^{\dagger} - C_{x,2}C_{y,1}^{\dagger} - C_{x,1}C_{y,2}^{\dagger})$.

We show the outline of the calculation the z-component of the Berry curvature (BC) for the α^{th} occupied band $\Omega_{xy}^{(\alpha)}(k) = 2 \text{Im}(-C_{x,1}C_{y,1}^{\dagger} + C_{x,2}C_{y,1}^{\dagger} + C_{x,1}C_{y,2}^{\dagger})$ here. We obtain

$$\begin{aligned} -2\text{Im}(C_{x,1}C_{y,1}^{\dagger}) = & 2N_{\alpha}^{-1} [-\partial_x Y_1^{(\alpha)} \partial_y Y_2^{(\alpha)} + \partial_x Y_2^{(\alpha)} \partial_y Y_1^{(\alpha)} - \partial_x \kappa_1^{(\alpha)} \partial_y \kappa_2^{(\alpha)} + \partial_x \kappa_2^{(\alpha)} \partial_y \kappa_1^{(\alpha)} \\ & - \partial_x \Delta_1^{(\alpha)} \partial_y \Delta_2^{(\alpha)} + \partial_x \Delta_2^{(\alpha)} \partial_y \Delta_1^{(\alpha)}], \quad (29) \end{aligned}$$

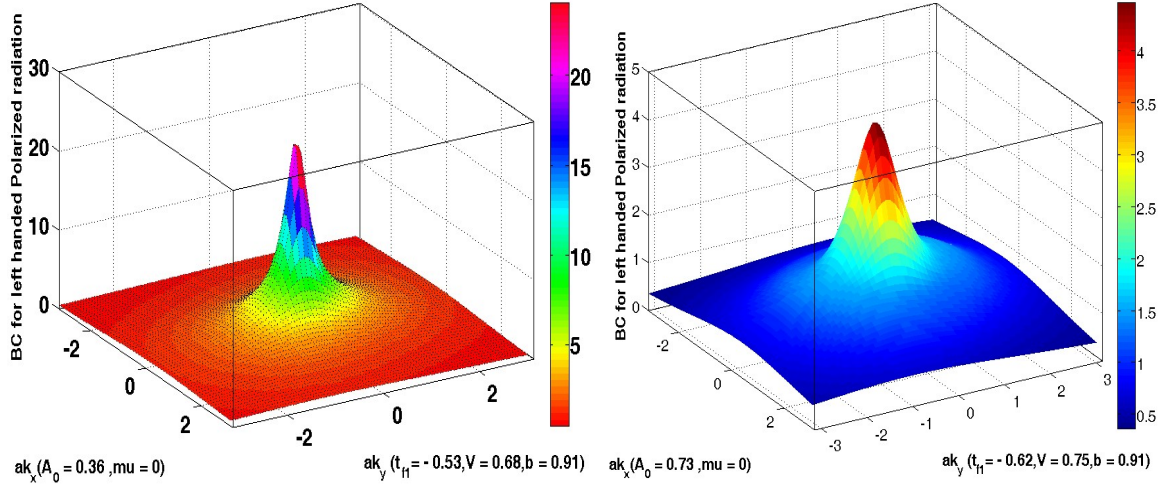
$$2 \operatorname{Im}(C_{x,2}C_{y,1}^\dagger) = N_\alpha^{-2}(\partial_x N_\alpha) [Y_1^{(\alpha)}\partial_y Y_2^{(\alpha)} - Y_2^{(\alpha)}\partial_y Y_1^{(\alpha)} + \kappa_1^{(\alpha)}\partial_y \kappa_2^{(\alpha)} - \kappa_2^{(\alpha)}\partial_y \kappa_1^{(\alpha)} \\ + \Delta_1^{(\alpha)}\partial_y \Delta_2^{(\alpha)} - \Delta_2^{(\alpha)}\partial_y \Delta_1^{(\alpha)}], \quad (30)$$

$$2 \operatorname{Im}(C_{x,1}C_{y,2}^\dagger) = N_\alpha^{-2}(\partial_y N_\alpha) [\partial_x Y_1^{(\alpha)}Y_2^{(\alpha)} - \partial_x Y_2^{(\alpha)}Y_1^{(\alpha)} + \partial_x \kappa_1^{(\alpha)}\kappa_2^{(\alpha)} - \partial_x \kappa_2^{(\alpha)}\kappa_1^{(\alpha)} \\ + \partial_x \Delta_1^{(\alpha)}\Delta_2^{(\alpha)} - \partial_x \Delta_2^{(\alpha)}\Delta_1^{(\alpha)}], \quad (31)$$

In view of (29) - (31), we obtain

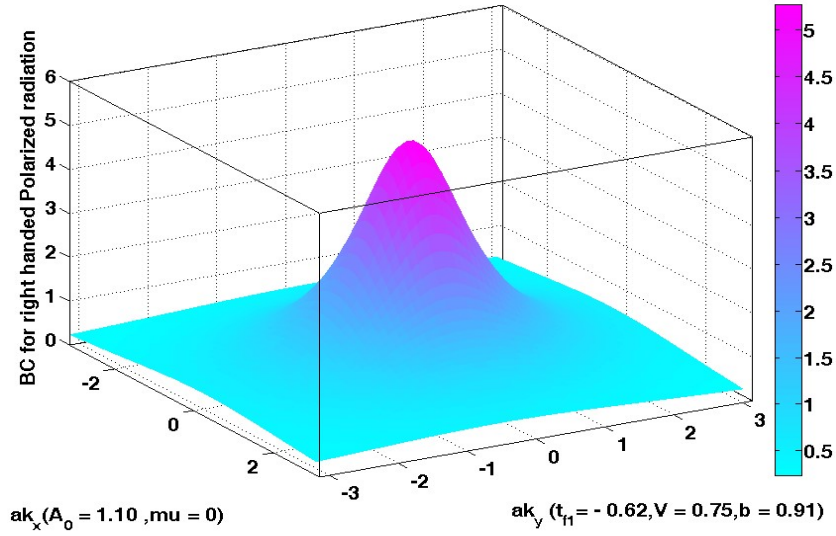
$$\Omega_{xy}^{(\alpha)}(k) = N_\alpha^{-1} [(\partial_y Y_1^{(\alpha)} - N_\alpha^{-1}(\partial_y N_\alpha)Y_1^{(\alpha)}) \partial_x Y_2^{(\alpha)} - (\partial_y Y_2^{(\alpha)} - N_\alpha^{-1}(\partial_y N_\alpha)Y_2^{(\alpha)}) \partial_x Y_1^{(\alpha)} \\ - N_\alpha^{-1} [(\partial_x Y_1^{(\alpha)} - N_\alpha^{-1}(\partial_x N_\alpha)Y_1^{(\alpha)}) \partial_y Y_2^{(\alpha)} - (\partial_x Y_2^{(\alpha)} - N_\alpha^{-1}(\partial_x N_\alpha)Y_2^{(\alpha)}) \partial_y Y_1^{(\alpha)}] \\ + N_\alpha^{-1} [(\partial_y \kappa_1^{(\alpha)} - N_\alpha^{-1}(\partial_y N_\alpha)\kappa_1^{(\alpha)}) \partial_x \kappa_2^{(\alpha)} - (\partial_y \kappa_2^{(\alpha)} - N_\alpha^{-1}(\partial_y N_\alpha)\kappa_2^{(\alpha)}) \partial_x \kappa_1^{(\alpha)}] \\ - N_\alpha^{-1} [(\partial_x \kappa_1^{(\alpha)} - N_\alpha^{-1}(\partial_x N_\alpha)\kappa_1^{(\alpha)}) \partial_y \kappa_2^{(\alpha)} - (\partial_x \kappa_2^{(\alpha)} - N_\alpha^{-1}(\partial_x N_\alpha)\kappa_2^{(\alpha)}) \partial_y \kappa_1^{(\alpha)}] \\ + N_\alpha^{-1} [(\partial_y \Delta_1^{(\alpha)} - N_\alpha^{-1}(\partial_y N_\alpha)\Delta_1^{(\alpha)}) \partial_x \Delta_2^{(\alpha)} - (\partial_y \Delta_2^{(\alpha)} - N_\alpha^{-1}(\partial_y N_\alpha)\Delta_2^{(\alpha)}) \partial_x \Delta_1^{(\alpha)}] \\ - N_\alpha^{-1} [(\partial_x \Delta_1^{(\alpha)} - N_\alpha^{-1}(\partial_x N_\alpha)\Delta_1^{(\alpha)}) \partial_y \Delta_2^{(\alpha)} - (\partial_x \Delta_2^{(\alpha)} - N_\alpha^{-1}(\partial_x N_\alpha)\Delta_2^{(\alpha)}) \partial_y \Delta_1^{(\alpha)}]. \quad (32)$$

Now that we have calculated a formal expression for the BC of α band, what remains to be done is to calculate various derivatives in (32). This is a lengthy but straightforward task. In Figure 3 we have shown the 3D plots of BC in the z -direction as a function of the wavenumber components (k_x, k_y) . The numerical values of the parameters used in the plots are $t_{d_1} = 1$, $t_{f_1} = -0.53/-0.62$, $t_{d_2} = 0.01$, $t_{f_2} = 0.01$, $t_{d_3} = 0.001$, $t_{f_3} = 0.001$, $V = 0.68/0.75$, $\epsilon_f = -0.02$, $q = 0.1$, $b = 0.91$, and $\mu = 0$. The amplitude of incident radiation aA_0 is 0.36 in Figure (a) whereas it is 0.73 in Figure (b). These figures correspond to left-handed circularly polarized light. Upon integrating BC on a k -mesh-grid of the Brillouin zone (BZ), we calculate the intrinsic anomalous Hall conductivity (AHC) σ_{AH} . This yields the Chern number (C). We find that AHC is $\sigma_{AH} = 2.0265 \left(\frac{e^2}{h}\right)$ ($C \approx 2.0265$) in the former case, while in the latter case it is $\sigma_{AH} = 1.0002 \left(\frac{e^2}{h}\right)$ ($C \approx 1$). Obviously enough, in the former case, the Chern number has non-integer value as this case corresponds to metallicity (see Figure 1(c)). We find that the increase in the intensity of the incident radiation gives rise to the integer value of the Chern number, though there is slight change in parameter values used to calculate the Chern number. In Figure 3(c) we have shown the 3D plot of BC in the z -direction for the right-handed circularly polarized radiation with $aA_0 = 1.10$. Here we obtain



(a) $C = 2.0265$

(b) $C = 1.0002$



(c) $C = 1.0008$

Figure 3. The 3D plots of the Berry curvature along z-direction as a function of the wavenumber components (k_x, k_y). The numerical values of the parameters used in the plots are $t_{d1} = 1$, $t_{f1} = -0.53/-0.62$, $t_{d2} = 0.01$, $t_{f2} = 0.01$, $t_{d3} = 0.001$, $t_{f3} = 0.001$, $V = 0.68/0.75$, $\epsilon_f = -0.02$, $q = 0.1$, $b = 0.91$, and $\mu = 0$. While the amplitude of incident radiation aA_0 is 0.36 in Figure (a), it is 0.73 in Figure (b). These figures correspond to left-handed circularly polarized light. In Figure(c) we have shown the 3D plot of BC in the z-direction for the right-handed circularly polarized radiation with $aA_0 = 1.10$.

$\sigma_{AH} = 1.0008 \left(\frac{e^2}{h} \right) (C \approx 1)$. It is worth mentioning that a higher value of the intensity of incident radiation indicates the possibility of the topological switching between the metallic state and the

QAH state. The sign of the term $C_3 = M$ in (1) does not seem to affect the value of the Chern number. That is, QAH effect is possible via periodically driven radiation in both the ferromagnetic (FM) and the anti-ferromagnetic (AFM) insulators. This is not quite surprising as there has been an attempt earlier to derive AFM Chern insulator from the Kane-Mele Hubbard model albeit in the non-centrosymmetric systems [32]. Furthermore, recently it has been shown [33] that a monolayer CrO can be switched from an AFM Weyl semimetal to an AFM QAH insulator by applying strain. Also, in the case of the AFM material MoO monolayer the shear strain, upon breaking the time reversal symmetry, drives the system to have nontrivial electronic bands with the magnitude of the Chern number as unity [34]. Since the Neel temperature of the system is above the room temperature, it may be useful in spintronics applications. As for the other practical uses, the energy-efficient electronic devices [35] and the multichannel quantum computing [36, 37] could be facilitated by such topologically switchable materials.

5. Concluding remarks

The original time-dependent problem (with periodicity in external driving force) could be mapped into effective time-independent formulation in Floquet theory [14-19]. The theory was used extensively in the past in the theoretical studies of external driving on transport in various systems commissioning combination of the theory with Schrodinger equation [38], Green's functions [39-41], quantum master equation [42,43], scattering matrix approach [44], and so on. The combinations of the Floquet theory with dynamical mean field theory [45], and slave boson protocol (SBP) [46] were also formulated for strongly correlated systems. Our approach in this paper is in acquiescence to the latter. In this article, we use a SBP version of the Periodic Anderson Hamiltonian in combination with the Floquet theory to develop a microscopic approach to study the effects of external perturbations like electromagnetic fields on the non-trivial topological surface properties of SmB₆. The surface state, obtained by the evanescent wave approach, is assumed to possess the comparable penetration depth like that in Bi₂Se₃. In the preceding sections we have shown that the periodic driving of circularly polarized light leads to a new avenue for obtaining novel QAH effect that may be inaccessible in static systems. For this purpose, the effective, static surface Hamiltonian (1) has been obtained using the high-frequency Floquet-Magnus expansion [19, 47-50]. These are the highlights of the article. It may be mentioned that In the high-frequency domain, other equivalent expansions such as van Vleck [51,52], or Brillouin-Wigner [53] could also be used to describe the system surface in terms of a time-independent Hamiltonian.

References

1. S. S. Dabiri, H. Cheraghchi, A. Sadeghi, *Phys. Rev. B* **103**, 205130 (2021).
2. H. Xu, J. Zhou, Ju Li, *Advanced Science*, 2101508 (2021).
3. W. Zhu, M. Umer, and J. Gong, *Phys. Rev. Research* **3**, L032026 (2021).

4. L. Zhou, C. Chen, and J. Gong, *Phys. Rev. B* 94, 075443 (2016).
5. H. Hubener, M. A. Sentef, U. De Giovannini, A. F. Kemper, and A. Rubio, *Nat. Commun.* 8, 13940 (2017).
6. D. Zhang, H. Wang, J. Ruan, G. Yao, and H. Zhang, *Phys. Rev. B* 97, 195139 (2018).
7. H. Liu, J.-T. Sun, and S. Meng, *Phys. Rev. B* 99, 075121 (2019).
8. L. Li, C. H. Lee, and J. Gong, *Phys. Rev. Lett.* 121, 036401 (2018).
9. X. Liu, P. Tang, H. Hübener, U. De Giovannini, W. Duan, and A. Rubio, *arXiv preprint arXiv:2106.06977* (2021).
10. F. Qin, R. Chen, and H.-Z. Lu, *J. Phys. Condens. Matter* 34, 225001 (2022).
11. J. W. McIver, B. Schulte, F.-U. Stein, T. Matsuyama, G. Jotzu, G. Meier, and A. Cavalleri, *Nature Physics* 16, 38 (2019).
12. B. K. Wintersperger, C. Braun, F. N. Unal, A. Eckardt, M. D. Liberto, N. Goldman, I. Bloch, and M. Aidelsburger, *Nature Physics* 16, 1058 (2020).
13. C. S. Afzal, T. J. Zimmerling, Y. Ren, D. Perron, and V. Van, *Phys. Rev. Lett.* 124, 253601 (2020).
14. H. Sambe, *Phys. Rev. A* 7, 2203 (1973).
15. A. A. Pervishko, D. Yudin, and I. A. Shelykh, *Phys. Rev. B* 97, 075420 (2018).
16. R. Chen, B. Zhou, and D.-H. Xu, *Phys. Rev. B* 97, 155152 (2018).
17. R. Chen, D.-H. Xu, and B. Zhou, *Phys. Rev. B* 98, 235159 (2018).
18. N. Goldman and J. Dalibard, *Phys. Rev. X* 4, 031027 (2014).
19. A. Eckardt and E. Anisimovas, *New J. Phys.* 17, 093039 (2015).
20. D. J. Kim, S. Thomas, T. Grant, J. Botimer, Z. Fisk, J. Xia, *Sci. Rep.*, 3, 3150(2013).
21. M. Dzero, K. Sun, V. Galitski, P. Coleman, *Phys. Rev. Lett.* 2010, 104, 106408(2010).
22. Partha Goswami, *Pramana – J. Phys.* 96:116 (2022).
23. Partha Goswami and Udai Prakash Tyagi, *arXiv: 2311.00583(cond-mat.mes-hall)*(2023).
24. Udai Prakash Tyagi, Kakoli Bera and Partha Goswami, *Symmetry*,13(12), 2245 (2021).
25. M. Legner, ETH Zurich Research Collection(2016).Link:<https://www.research-collection.ethz.ch/bitstream/handle/20.500.11850/155932/eth-49918-02.pdf?isAllowed=y&sequence=2>.
26. J Betancourt, S. Li, X. Dang, J. D. Burton, E. Y. Tsymbal, and J. P. Velev, *J. Phys.: Condens. Matter* 28 395501(2016).
27. F. Lu, J. Zhou Zhao, H. Weng, Z. Fang, Xi Dai, *Phys. Rev. Lett.* 110, 096401 (2013).
28. M. V. Berry, *Proc. Roy. Soc. Lond. A* 392, 45 (1984).
29. G. D. Mahan, *Many-particle physics (Springer Science and Business Media)*(2013).
30. D. J. Thouless, M. Kohmoto, M. P. Nightingale, and M. den Nijs, *Phys. Rev. Lett.* 49, 405(1982).
31. Q. Niu, D. J Thouless, and Y.-S. Wu, *Phys. Rev. B* 31, 3372 (1985).
32. K. Jiang, S. Zhou, X. Dai, and Z. Wang, *Phys. Rev. Lett.* 120, 157205 (2018).
33. P.J. Guo, Z. X. Liu, and Z.Y. Lu, *NPJ Comput. Mater* 9, 70 (2023).
34. B. Wu, Y.-L. Song, W.-X Ji, P.-J. Wang, S.-F. Zhang, and C.-W. Zhang, *Phys. Rev. B* 107, 214419 (2023).
35. K. He, Y. Wang, and Q.-K. Xue, *Annual Review of Condensed Matter Physics* 9, 329 (2018).
36. Q. L. He, L. Pan, A. L. Stern, E. C. Burks, X. Che, G. Yin, J. Wang, B. Lian, Q. Zhou, E. S. Choi, et al., *Science* 357, 294 (2017).

37. J. Wang, Q. Zhou, B. Lian, and S.-C. Zhang, *Phys. Rev. B* 92, 064520 (2015); K. He, Y. Wang, and Q.-K. Xue, *Annual Review of Condensed Matter Physics* 9, 329 (2018).
38. D. Thuberg, E. Muñoz, S. Eggert, and S. A. Reyes, *Phys. Rev. Lett.* 119, 267701 (2017).
39. G. Stefanucci, S. Kurth, A. Rubio, and E. K. U. Gross, *Phys. Rev. B* 77, 075339 (2008).
40. B. H. Wu and J. C. Cao, *J. Phys.: Condens. Matter* 20, 085224 (2008).
41. D. Rai and M. Galperin, *J. Phys. Chem. C* 117, 13730 (2013).
42. J. Lehmann, S. Kohler, P. Hnggi, and A. Nitzan, **Phys. Rev. Lett.** 88, 228305 (2002).
43. B. H. Wu and C. Timm, *Phys. Rev. B* 81, 075309 (2010).
44. B. H. Wu and J. C. Cao, *Phys. Rev. B* 73, 245412 (2006).
45. N. Tsuji, T. Oka, and H. Aoki, *Phys. Rev. B* 78, 235124 (2008).
46. B. H. Wu and J. C. Cao, *Phys. Rev. B* 81, 085327 (2010).
47. W. Magnus, *Communications on pure and applied mathematics* 7, 649 (1954).
48. S. Blanes, F. Casas, J.-A. Oteo, and J. Ros, *Physics reports* 470, 151 (2009).
49. M. Bukov, L. D'Alessio, and A. Polkovnikov, *Advances in Physics* 64, 139 (2015).
50. C. H. Lee, W. W. Ho, B. Yang, J. Gong, and Z. Papić, *Phys. Rev. Lett.* 121, 237401 (2018).
51. H. Xu, J. Zhou, and J. Li, *Advanced Science* 8, 2101508 (2021).
52. S. S. Dabiri and H. Cheraghchi, **Phys. Rev. B** 104, 245121 (2021).
53. T. Mikami, S. Kitamura, K. Yasuda, N. Tsuji, T. Oka, and H. Aoki, *Phys. Rev. B* 93, 144307 (2016).

Statement Regarding Data Analyzed : All data used or analyzed during this study are included in this article.

Appendix A

The evanescent approach involves making the ansatz that the corresponding states are quasi-localized within the surface $z = 0$ of the form $\exp\left(-\frac{z}{d}\right) |u^{(\alpha)}(k)\rangle$ for $z > 0$ and $\exp\left(-\frac{|z|}{d}\right) |u^{(\alpha)}(k)\rangle$ for $z < 0$, where $k = \sqrt{k_x^2 + k_y^2}$, $|u^{(\alpha)}(k)\rangle$ is eigenstate of α^{th} band of the surface Hamiltonian $h_f(k_x, k_y, \mu, b)$ given below and d is the surface-state penetration depth. For a value $d \sim 5-10$ nm as in Bi_2Se_3 , $\frac{a}{d} \sim 0.08 - 0.05$ (the lattice constant of SmB_6 is $a = 0.413$ nm) which ensures that the decaying term $\exp\left(-\frac{z}{d}\right)$ and $\exp\left(-\frac{|z|}{d}\right) \sim \exp(-1)$ for $|z| \sim 5-10$ nm. We consider below this case. Next, we make the replacement $ak_z \rightarrow -ia \partial_z$ in (1) as the z -component of the momentum (eigenvalue) is not a good quantum number. Upon differentiation, the third component of ϑ_μ in (1) appears as $(2Vb \sin\left(\frac{a}{d}\right))$.

We now treat the model Hamiltonian matrix in (1) in the low-energy limit near $\bar{\Gamma}(0,0)$ point. In this limit, using Taylor expansion we write $\sin(ak_j) \rightarrow ak_j + O(a^3 k_j^3)$, $\cos(ak_j) \rightarrow (1 - \frac{1}{2}a^2 k_j^2) + O(a^4 k_j^4)$, $j = (x, y)$. Moreover, one may approximate $\sin(a/d)$ by $\left(\frac{a}{d} -$

$\frac{(a/d)^3}{3!} + \dots$) and $\cos(a/d)$ by $(1 - \frac{(a/d)^2}{2} + \dots)$. The low-energy surface Hamiltonian can now be conveniently written as $h_f = \frac{\epsilon(k,d,\mu,b) + \vartheta(k,b,d)}{2} (I^{4 \times 4} + \gamma^0) + \frac{\epsilon(k,d,\mu,b) - \vartheta(k,b,d)}{2} (I^{4 \times 4} - \gamma^0) + iA_1 a k_x \gamma^2 + A_1 a k_y \gamma^0 \gamma^2 - iA_1 (\frac{a}{d}) \gamma^3$, where $A_1 = 2Vb$. In the low-energy limit, the functions $\epsilon(k,\mu,d,b) = \frac{(\widetilde{E}_k^d(\mu,k) + \widetilde{E}_k^f(\mu,b,k))}{2}$ and $\vartheta(k,\mu,d,b) = \frac{(\widetilde{E}_k^d(\mu,k) - \widetilde{E}_k^f(\mu,b,k))}{2}$ have been approximated to $O(a^2 k^2)$. The dispersions in section 2 are given by the expressions $\widetilde{E}_k^d(\mu,k) = -\mu + 3t_{d1} - 3t_{f1} - \mathfrak{h}_d$ and $\widetilde{E}_k^f(\mu,b,k) = -\mu - 3t_{d1} - 3t_{f1} + b^2(\epsilon_f + 6t_{f1}) - b^2 \mathfrak{h}_f$, where $\mathfrak{h}_d = [2t_{d1} c_1(k) + 4t_{d2} c_2(k) + 8t_{d3} c_3(k)]$, $\mathfrak{h}_f = [2t_{f1} c_1(k) + 4t_{f2} c_2(k) + 8t_{f3} c_3(k)]$, $c_1(k) = \sum_{\mu} \cos(ak_{\mu})$, $c_2(k) = \sum_{\mu \neq \nu} (\cos k_{\mu} a \cdot \cos k_{\nu} a)$, and $c_3(k) = \prod_{\mu} (\cos k_{\mu} a)$, $\mu = (x, y, z)$. In the low-energy limit, the functions $\epsilon(k,\mu,d,b)$ and $\vartheta(k,\mu,d,b)$ appearing in section 2 could be approximated as

$$\epsilon(k,d,\mu,b) = \epsilon_0(\mu,b) - D_1(b)a^2 d^{-2} + D_2(b)a^2 k^2 + O(a^4 d^{-4}) + O(a^4 k^4), \quad (\text{A.1})$$

$$\vartheta(k,d,b) = \vartheta_0(b) - B_1(b)a^2 d^{-2} + B_2(b)a^2 k^2 + O(a^4 d^{-4}) + O(a^4 k^4), \quad (\text{A.2})$$

$$\epsilon_0(\mu,b) = -\mu + [\frac{b^2}{2}\epsilon_f - 3t_{d1} - 3t_{f1} - 6t_{d2} - 6t_{f2}b^2 - 4t_{d3} - 4t_{f3}b^2], \quad (\text{A.3})$$

$$D_1(b) = D_2(b) = [\frac{t_{d1} + b^2 t_{f1}}{2} + 2(t_{d2} + b^2 t_{f2}) + 2(t_{d3} + b^2 t_{f3})], \quad (\text{A.4})$$

$$\vartheta_0(b) = [-\frac{b^2 \epsilon_f}{2} - 6t_{d2} + 6t_{f2}b^2 - 4t_{d3} + 4t_{f3}b^2], \quad (\text{A.5})$$

$$B_1(b) = B_2(b) = [\frac{t_{d1} - b^2 t_{f1}}{2} + 2(t_{d2} - b^2 t_{f2}) + 2(t_{d3} - b^2 t_{f3})]. \quad (\text{A.6})$$

It may be mentioned in passing that in the case $d \sim 0.13 \text{ nm} < a$ (lattice constant) $\sim 0.4 \text{ nm}$, we obtain $\frac{a}{d} \sim 3.1416 \dots \sim \pi$. Consequently, $e^{-|z|/d}$ will be nearly equal to e^{-1} for very low value of $|z|$ ($\sim 0.1 \text{ nm}$). We shall refer to this as the low penetration depth (LPD) case. We can present the Hamiltonian (1) in the basis $(d_{k,\uparrow} \ bc_{k,\downarrow} \ d_{k,\downarrow} \ bc_{k,\uparrow})^T$ in the non-block-diagonal form:

$$\begin{pmatrix} \epsilon_{OP} + \vartheta_{OP}^+ & A_{1OP}^+(ak_-) & 0 & -iA_{1OP}^+(aq) \\ A_{1OP}^+(ak_+) & \epsilon_{OP} - \vartheta_{OP}^+ & -iA_{1OP}^-(aq) & 0 \\ 0 & iA_{1OP}^-(aq) & \epsilon_{OP} + \vartheta_{OP}^- & -A_{1OP}^-(ak_-) \\ iA_{1OP}^-(aq) & 0 & -A_{1OP}^-(ak_+) & \epsilon_{OP} - \vartheta_{OP}^- \end{pmatrix} \quad (\text{A.7})$$

Since in the LPD case the terms like $(iA_{10P}^\pm(aq))$ will be absent, Eq. (A.7) assumes a block-diagonal form in this case. The energy eigenvalues for the block-diagonal are

$$\mathcal{E}_\mu(s, k, b, I) = \epsilon_{OP}(k, b) \pm \sqrt{[\vartheta_{OP}^{(\mu)^2} + A_{10P}^{(\mu)^2} ((ak_x)^2 + (ak_y)^2)]} \quad (\text{A.8})$$

where the index $\mu = +1(-1)$ for the left-handed (right-handed) circularly polarized radiation, respectively. The corresponding eigenvectors could be obtained from Eq. (16)-(23) dropping (aq)

involving terms. Upon using the formula $\Omega_{xy}(k) = -2 \sum_\alpha \text{Im} \left\langle \frac{\partial u^{(\alpha)}(k)}{\partial k_x} \middle| \frac{\partial u^{(\alpha)}(k)}{\partial k_y} \right\rangle$, it is not difficult to obtain the result $\Omega_{xy}(k) = \sum_\alpha \Omega_{xy}^{(\alpha)}(k)$ where

$$\Omega_{xy}^{(\alpha)}(k) = N_\alpha^{-1} (A_{10P}^{+2} + A_{10P}^{-2}) [(1 - N_\alpha^{-1} \partial_x N_\alpha(ak_x)) + (1 - N_\alpha^{-1} \partial_y N_\alpha(ak_y))], \quad (\text{A.9})$$

and $N_\alpha = [(A_{10P}^{+2} + A_{10P}^{-2}) ((ak_x)^2 + (ak_y)^2) + (\mathcal{E}_\alpha - \epsilon_{OP} - \vartheta_{OP}^+)^2 + (\mathcal{E}_\alpha - \epsilon_{OP} - \vartheta_{OP}^-)^2]$.

Appendix B

Analogous to the Bloch theory involving quasi-momentum, a solution/wave function $|\psi(t)\rangle = e^{-i\epsilon t} |\psi_f(t)\rangle$ involving the Floquet quasi-energy ϵ could be written down for the time-dependent Schrodinger equation of the system, where the Floquet state satisfies $|\psi_f(t)\rangle = |\psi_f(t+T)\rangle$. The periodicity implies that $|\psi_f(t)\rangle$ could be expanded in a Fourier series: $|\psi_f(t)\rangle = \sum_r \exp(-ir\omega t) |\psi_f^r\rangle$ where r is an integer. Then the wave function $|\psi(t)\rangle$, in terms of the quasi-energy ϵ , has the form $|\psi(t)\rangle = \sum_r \exp\left(-i\left(\frac{\epsilon}{\hbar} + r\omega\right)t\right) |\psi_f^r\rangle$. This makes us arrive at an infinite dimensional eigenvalue equation in the Sambe space (the extended Hilbert space)[26]: $\sum_r h_{f,r,s} |\psi_{f,n}^s\rangle = \epsilon_n |\psi_{f,n}^s\rangle$. The matrix element $h_{f,\alpha,\beta}$ is given by $h_{f,\alpha,\beta} = \alpha\hbar\omega\delta_{\alpha,\beta} + \frac{1}{T} \int_0^T h_f(t) e^{i(\alpha-\beta)\omega t} dt$, where (α, β) are integers. This is the Floquet surface state Hamiltonian matrix element. In view of the Floquet theory [14-19], we can now write a static effective Hamiltonian $H_f^{\text{Floquet}}(k, d, aA_0, \mu, b)$, in the off-resonant regime using the Floquet-Magnus expansion [17]: $H_f^{\text{Floquet}}(k, d, aA_0, \mu, b) = h_{f,0,0} + \frac{[h_{f,0,-1}, h_{f,0,1}]}{\hbar\omega} + O(\omega^{-2})$, where $h_{f,n,m} = \frac{1}{T} \int_0^T h_f(t) e^{i(n-m)\omega t} dt$ with $n \neq m$. In the low-energy and high frequency limit, the terms $h_{f,0,0}$ is given by $h_{f,0,0} = h_f(k, q, \mu, b) + D_1(b)(a^2 A_0^2) I_{4 \times 4} + B_1(b) (a^2 A_0^2) \sigma_{12}$. The remaining two terms $h_{f,0,1}$ and $h_{f,0,-1}$ are polarization handedness dependent, e.g. $h_{f,0,1} = iD_1(b)\chi I^{4 \times 4} + iB_1(b)\chi \sigma_{12} + (i/2) A_1(aA_0) \sigma_{23} + (i/2) A_1(aA_0) e^{i\psi} \sigma_{31}$, $\chi = a^2 (k_x + e^{i\psi} k_y) A_0$. The term $h_{f,0,-1}$ could be obtained replacing i by $(-i)$ in $h_{f,0,1}$. Here $\sigma_{\nu\rho} = \left(\frac{i}{2}\right) [\gamma_\nu, \gamma_\rho]$, and the covariant form $\gamma_\mu = \eta_{\mu\nu} \gamma^\nu = (\gamma^0, -\gamma^1, -\gamma^2, -\gamma^3, \gamma^5)$. These commutators are expressible in terms of the tensor product of Pauli matrices in the orbital-spin basis. While $\sigma = (\sigma_x, \sigma_y, \sigma_z)$ acts on the real spin, $\tau = (\tau_x, \tau_y, \tau_z)$ acts on the orbital degree of freedom. The matrices τ and σ are acting together in the space of bands yielding spectral gaps in Figure 1.

We can write the (anti-unitary) time-reversal operator $\Theta = UK$ where U is a unitary operator. Furthermore, for a spin-1/2 particle, flipping the spin coincides with the time-reversal. This means $\Theta \hat{\mathcal{S}} = -\hat{\mathcal{S}}$ where $\hat{\mathcal{S}} = \frac{1}{2} \hat{\boldsymbol{\sigma}}$ and $\hat{\boldsymbol{\sigma}}$ is the vector of Pauli matrices. In view of these, one may choose $\Theta = i\tau_0 \otimes \sigma_y K$, where τ_0 is the identity matrix. The operator K stands for the complex conjugation. Upon making use of the results $\Theta \hat{A} \Theta^{-1} = \hat{A}$, $\Theta \hat{B} \Theta^{-1} = -\hat{B}$, and so on, where $\hat{A} = \tau_0 \otimes \sigma_0, \tau_z \otimes \sigma_y, \dots$ and $\hat{B} = \tau_0 \otimes \sigma_y, \dots$, we find that $\Theta H_f^{Floquet}(ak_x, ak_y, b, aA_0) \Theta^{-1} = H_f^{Floquet}(-ak_x, -ak_y, b)$ only when $\psi = 0$ or π , that is, when the radiation field is linearly polarized. Thus, for the linearly polarized radiation, the time reversal symmetry (TRS) is not broken. However, when $\psi = \frac{\pi}{2}$ or $-\frac{\pi}{2}$, that is the radiation is circularly polarized, TRS is broken. The reason being in these cases

$$\Theta H_f^{Floquet}(ak_x, ak_y, b, aA_0) \Theta^{-1} = H_f^{Floquet}(-ak_x, -ak_y, b) + (4a^2 A_0^2 \sin\psi / \hbar\omega) \times \\ \{A_1 ak_x \tau_0 \otimes \sigma_x + A_1 ak_y \tau_0 \otimes \sigma_y\} D_1(b) + \left(\frac{4a^2 A_0^2 A_1^2 \sin\psi}{\hbar\omega} \right) \tau_0 \otimes \sigma_z, \quad (\text{B.1})$$

We have adopted the same basis as in the appendix A to write (B.1). As shown above, due to the broken TR symmetry, this system can be regarded as a Chern insulator- a TR symmetry broken topological insulator with a non-zero Chern number. Furthermore, the inversion symmetry (IS) operator $\mathcal{I} = \tau_0 \otimes \sigma_z$ in the orbital – spin basis. We find that $\mathcal{I} \gamma^0 \mathcal{I}^{-1} = \gamma^0$, $\mathcal{I} \gamma^j \mathcal{I}^{-1} = -\gamma^j$ ($j = 1, 2$), and $\mathcal{I} \gamma^k \mathcal{I}^{-1} = \gamma^k$ ($k = 3, 5$). Since only γ^0 and γ^3 are even under inversion, it is clear that the Floquet Hamiltonian $H_f^{Floquet}$ in (1) breaks IS. The immediate consequences of this is the spin non-degeneracy of the bands, and the accessibility of the Berry curvature dipole (BCD), which is the first-order moment of Berry curvature (BC). It is worthwhile to note here that in the absence of spin-orbit interaction the Anderson model is both time reversal and inversion symmetric.